Inorganic Chemistry
Article
Cite This: Inorg. Chem. XXXX, XXX, XXX−XXX
pubs.acs.org/IC

Construction of Metallosupramolecular Coordination Complexes: From Lanthanide Helicates to Octahedral Cages Showing Single-Molecule Magnet Behavior

Yu Zhang,[†,‡] Basharat Ali,[†,§] Jianfeng Wu,[†] Mei Guo,[†] Yang Yu,*[,†] Zhiliang Liu,*[,‡] and Jinkui Tang*[,†,§]

[†]State Key Laboratory of Rare Earth Resource Utilization, Changchun Institute of Applied Chemistry, Chinese Academy of Sciences, Changchun 130022, PR China

[‡]College of Chemistry and Chemical Engineering, Inner Mongolia University, Hohhot 010021, PR China

[§]University of Science and Technology of China, Hefei 230026, PR China

Supporting Information

ABSTRACT: The construction of metallosupramolecular complexes toward interesting topological structures is a critical challenge for chemists. The fluctuation in the synthetic strategy, by keeping the same metal−ligand combination, has proved a very significant approach to construct metallosupramolecular architectures. Herein, by varying the reaction conditions four new Dy^{III}-supramolecular complexes based on a flexible dihydrazone ligand H_2L (H_2L = bis(2-hydroxy-3-methoxybenzylidene)adipohydrazide) in cooperation with different anions and solvents having formulas $[Dy_4L_4(\mu_2\text{-}N_3)_2](NO_3)_2\cdot 6CH_3OH\cdot 2H_2O$ (**1**), $[Dy_8L_8(\mu_2\text{-}CH_3OH)_4]Cl_8\cdot 6CH_3OH\cdot 14H_2O$ (**2**), $[Dy_{12}L_{12}(\mu_2\text{-}OH)_2(OH)_6(CH_3O)_2](NO_3)_2\cdot 2CH_3OH\cdot 14H_2O$ (**3**), and $[Dy_{12}L_{12}(\mu_2\text{-}OH)_2(NO_3)_2(OH)_3(CH_3O)](NO_3)_4\cdot 22H_2O$ (**4**), have been successfully synthesized and their crystal structures confirmed by single crystal X-ray diffraction studies. The structural study reveals that **1** and **2** have quadruple-stranded helicate and dual triple-stranded helicate supramolecular structures, respectively, while **3** and **4** display "octahedron" cagelike supramolecular structures. The magnetic studies reveal that complexes **1**−**3** exhibit slow magnetic relaxation behavior, while complex **4** displays a series of typical frequency-dependent relaxation signals at 0 Oe applied dc field which is a rare case in polynuclear 4f single-molecule magnet (SMM) family to date. Interestingly, the distinct magnetic dynamic behavior was noticed for nearly isoskeletal complexes **3** and **4**, which can be attributed to the modification of the coordination environment around Dy^{III} ions.

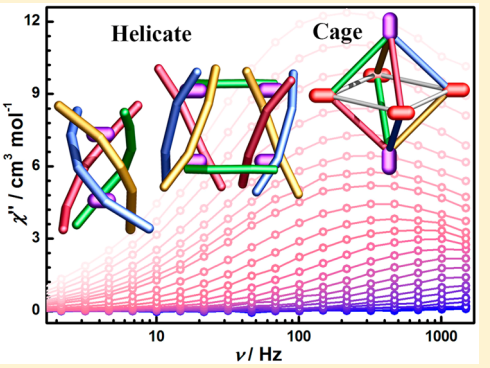

INTRODUCTION

Synthetic inorganic chemistry continues to obtain novel metal complexes that recently have lifted the field of modern inorganic self-assembly supramolecular coordination complexes with a variety of fascinating structural and physical properties.[1] Over the last couple of decades, quite a few chemists have thrived on exploring variety of available synthetic strategies to assemble supramolecular architectures in a steerable manner.[2] Up to now, by alternating the coordination environments around central metal ions and appropriate selection of organic ligands have constructed many well-defined supramolecular structures,[2c] such as rotaxanes,[3] interlocks,[4] catenanes,[5] rings,[6] helicates,[7] grids,[8] and cages,[9] showing stunning and multifunctional properties. In particular, the design and synthesis of helicate-, grid-, and cagetype metallosupramolecular complexes have attracted much attention from chemists, physicists and materials scientists.

Usually, most of explorations were focused on 3d metal complexes and have been acquired with remarkable success; hundreds of thousands of supramolecular architectures appear on the scene, which exhibit various sizes and interesting topological structures with potential applications including in gas storage and separation,[10] catalysis,[11] recognition and adsorption of sensitive guest molecules.[12] By contrast, lanthanide-containing polynuclear complexes were not developed to such an extent.[13] In view of the unique physical and chemical characteristics, lanthanide complexes play an indispensable role in modern inorganic supramolecular chemistry and create a wide range of exceptional values.[14] Despite this versatility, lanthanide ions also possess a large ionic radius and intricate and mutable coordination numbers and geometries, which brew a new endeavor and unparalleled challenge for introducing lanthanide elements into the supramolecular system.[15]

Among a wealth of architectures, a prominent position is held by helicate- and cagetype complexes. The chemistry of such kinds of molecules has been widely studied with a focus

Received: November 21, 2018

DOI: 10.1021/acs.inorgchem.8b03249
Inorg. Chem. XXXX, XXX, XXX−XXX

on the exploration of the topological structures. Except for geometrical descriptions, charming magnetic and luminescent behaviors are gaining increasing attention in lanthanide supramolecular complexes.[16] However, the coordination-driven self-assembly of lanthanide supramolecular structures is not easy to obtain owing to high kinetic lability of the Ln^{III} ions. Bearing this challenging task in mind, the judicious choice of different organic ligands incorporation with lanthanide ions might play a crucial role in course of exploring the unique supramolecular architectures. As a part of our research interest in the supramolecular chemistry field, we have long been developing tailored ligands as a linker that is able to construct various lanthanide supramolecular complexes, especially for Dy^{III} complexes,[17] which not only display beauteous topological structures but also endow excellent magnetic behaviors. Indeed, Dy^{III} ions with an large inherent magnetic anisotropy was deemed to be ideal candidates for the construction of ground-breaking results,[18] such as the new benchmark in molecular magnetism, $[(Cp^{iPr5})Dy(Cp^*)]^+$, which thus has pushed the anisotropic energy barriers record to 1541 cm^{-1}.[19] However, many endeavors have been dedicated toward the construction of polynuclear Ln-based complexes with the aim to obtain high-performance single-molecule magnets (SMMs), but supramolecular lanthanide complexes are still rare. Therefore, it is highly desirable to study the magnetic and structural characteristics of the supramolecular lanthanide complexes.

In the present work, we designed a flexible dihydrazone based ligand H_2L, in which two tetradentate pockets (ONOO) positioned at each side can effectively capture 4f ions. In addition, the middle of H_2L comprises a four membered $-CH_2-$ chain, which imparts extraordinary pliability and maneuverability for the ligand. Very recently, Liu and co-workers have reported a series of helicates by using an analogous ligand H_2L' with a two membered $-CH_2-$ chain.[7d] Later, the magnetic behaviors of isostructural complexes were published by Konar and co-workers.[20] Contrast to previous H_2L', the incorporation of the flexible spacers ($-C_4H_8-$) allows the ligand to better twist, rotate, bend, and so on in a proper way, which plays a significant role in developing supramolecular complexes.

Initially, by employing this flexible H_2L, a novel dysprosium based quadruple-stranded helicate supramolecular complex formulated as $[Dy_4L_4(\mu_2\text{-}N_3)_2](NO_3)_2{\cdot}6CH_3OH{\cdot}2H_2O$ (**1**) was obtained. The quadruple-stranded helicate complex **1** shows very similar structural features with analogs $[La_4L'_4(NO_3)](NO_3)_3$ previously reported by Liu's group.[7d] However, we find that by adjusting the reaction conditions the versatility of H_2L with Dy^{III} ion yielded the modification of quadruple-stranded helicate to dual triple-stranded helicate and octahedron cages (Scheme 1). Therefore, we further described the self-assembly of $[Dy_8L_8(\mu_2\text{-}CH_3OH)_4]Cl_8{\cdot}6CH_3OH{\cdot}14H_2O$ (**2**), $[Dy_{12}L_{12}(\mu_2\text{-}OH)_2(OH)_6(CH_3O)_2](NO_3)_2{\cdot}2CH_3OH{\cdot}14H_2O$ (**3**), and $[Dy_{12}L_{12}(\mu_2\text{-}OH)_2(NO_3)_2(OH)_3(CH_3O)](NO_3)_4{\cdot}22H_2O$ (**4**), demonstrating a structural evolution of the Dy^{III}-containing supramolecular architectures from helicates to cages.

It is generally known that Dy^{III} ions always grant an extraordinary magnetic anisotropy to the system. The distinctive topological and coordination environments exposed by all **1**–**4** complexes further inspired us to undertake a careful insight into their magnetic dynamics. Consequently, the alternating-current (ac) magnetic susceptibility measurements

Scheme 1. Schematic Representation of the Assembly of Supramolecular Dy_4L_4 (1), Dy_8L_8 (2) Helicates, and $Dy_{12}L_{12}$ (3 and 4) Cages

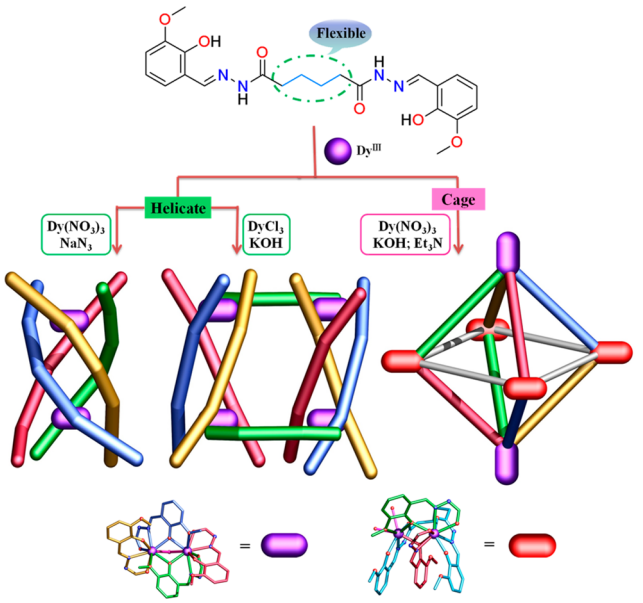

revealed complexes **1**–**3** as showing merely temperature-dependent slow magnetic relaxation behavior, while complex **4** displays typical frequency-dependent single-molecule magnet (SMM) behavior at 0 Oe applied field. In only a few studies,[21] the Ln-SMMs possessing 10 or more nuclearities have been discovered such as $[Dy_{14}(EDDC)_4(opch)_4(O_3PC_{10}H_7)_{10}(OAc)_6(H_2O)_4]{\cdot}xH_2O$.[21c]

EXPERIMENTAL SECTION

Synthesis of the Ligand. Ligand H_2L was prepared as previously reported.[22] A mixture of adipic dihydrazide (5 mmol, 0.87 g) and 3-methoxysalicylaldehyde (10 mmol, 1.52 g) in 100 mL of methanol was refluxed at 90 °C for 48 h. Then, the white precipitates were filtered and dried under vacuum to give H_2L. Yield: 1.51 g (68%). Elemental analysis (%) calcd for $C_{22}H_{26}N_4O_6$ (MW = 442.472): C, 59.72; H, 5.92; N, 12.66. Found: C, 59.68; H, 5.94; N, 12.69.

Synthesis of $[Dy_4L_4(\mu_2\text{-}N_3)_2](NO_3)_2{\cdot}6CH_3OH{\cdot}2H_2O$ (1). $Dy(NO_3)_3{\cdot}6H_2O$ (0.1 mmol, 45.6 mg) was added to a solution of H_2L (0.1 mmol, 44.2 mg) in 15 mL of CH_3OH/CH_3CN (v/v = 1:2), and then NaN_3 (0.2 mmol, 13.0 mg) was added. The resulting lemon-yellow suspension was stirred until turned clear and subsequently filtered. The filtrate was left undisturbed to allow the slow evaporation of the solvent at room temperature. After 1 week, yellow quadrate crystals of **1** were obtained in 21% yield (based on Dy salt). Elemental analysis (%) calcd for $C_{94}H_{96}Dy_4N_{24}O_{38}$ (MW = 2819.94): C, 40.04; H, 3.43; N, 11.92. Found: C, 40.14; H, 3.49; N, 11.81.

Synthesis of $[Dy_8L_8(\mu_2\text{-}CH_3OH)_4]Cl_8{\cdot}6CH_3OH{\cdot}14H_2O$ (2). $DyCl_3{\cdot}6H_2O$ (0.1 mmol, 37.6 mg) was added to a solution of H_2L (0.1 mmol, 44.2 mg) in 15 mL of CH_3OH/CH_3CN (v/v = 1:2), and then KOH (0.2 mmol, 5.61 mg) was added. After being stirred in air for 20 min, the resulting solution was transferred to a 20 mL reaction vial and heated to 80 °C for 2 h. Gradually cooling (3 °C/h) to room temperature, faint yellow clavate crystals of **2** were obtained in about 10% yield (based on Dy salt). Elemental analysis (%) calcd for $C_{186}H_{204}Cl_8Dy_8N_{32}O_{72}$ (MW = 5623.40): C, 39.73; H, 3.66; N, 7.97. Found: C, 39.82; H, 3.71; N, 7.92.

Synthesis of $[Dy_{12}L_{12}(\mu_2\text{-}OH)_2(OH)_6(CH_3O)_2](NO_3)_2{\cdot}2CH_3OH{\cdot}14H_2O$ (3). $Dy(NO_3)_3{\cdot}6H_2O$ (0.1 mmol, 44.2 mg) was added to a solution of H_2L (0.1 mmol, 44.2 mg) in 15 mL of CH_3OH/CH_3CN (v/v = 1:2), and then KOH (0.2 mmol, 5.61 mg) was added. The resulting lemon-yellow suspension was stirred until clear and

DOI: 10.1021/acs.inorgchem.8b03249
Inorg. Chem. XXXX, XXX, XXX−XXX

subsequently filtered. The filtrate was left undisturbed to allow the slow evaporation of the solvent at room temperature. Yellow clavate crystals of **3** were obtained after 10 days in relatively good yield (≈33%, based on Dy salt). Elemental analysis (%) calcd for $C_{268}H_{294}Dy_{12}N_{50}O_{104}$ (MW = 7829.51): C, 41.11; H, 3.78; N, 8.94. Found: C, 41.19; H, 3.83; N, 8.89.

Synthesis of $[Dy_{12}L_{12}(\mu_2\text{-}OH)_2(NO_3)_2(OH)_3(CH_3O)](NO_3)_4\cdot 22H_2O$ (4). $Dy(NO_3)_3\cdot 6H_2O$ (0.1 mmol, 44.2 mg) was added to a solution of H_2L (0.1 mmol, 44.2 mg) in 15 mL of CH_3OH/CH_3CN (v/v = 1:2), and then Et_3N (0.2 mmol, 28 μL) was added. The resulting lemon-yellow suspension was stirred until become clear and subsequently filtered. The filtrate was left undisturbed to allow the slow evaporation of the solvent at room temperature. Yellow clubbed crystals of **4** were obtained after 10 days in about 24% yield (based on Dy salt). Elemental analysis (%) calcd for $C_{265}H_{292}Dy_{12}N_{54}O_{119}$ (MW = 8087.51): C, 39.35; H, 3.64; N, 9.35. Found: C, 39.26; H, 3.67; N, 9.41.

RESULTS AND DISCUSSION

Synthetic Aspects. The dihydrazone-based ligand H_2L with extremely flexible characteristic can construct stable complex structure. However, the assembly process of lanthanide complexes is very sensitive to reaction conditions. In the present work, we explores the distinctive anions/bases-dependence that controls the assembly of H_2L and Dy^{III} ions (Scheme 1). A quadruple-stranded helicate structure was obtained using H_2L, $Dy(NO_3)_3\cdot 6H_2O$, and NaN_3. Using $DyCl_3\cdot 6H_2O$ and KOH instead of $Dy(NO_3)_3\cdot 6H_2O$ and NaN_3, a dual triple-stranded helicate structure was achieved. Meanwhile, only the KOH or Et_3N was used in place of NaN_3; two octahedral cage structures were assembled. This fascinating evolution inspired us to study the crystal structures and magnetic behaviors.

Crystallography. The yellow single crystals of complexes **1**−**4** were obtained from the reaction of H_2L with hydrated salts of dysprosium incorporate with corresponding bridging secondary ligands (for details, see the Experimental Section). Single-crystal X-ray diffraction analysis revealed that **1**−**3** crystallized in the monoclinic space group $C2/c$, and **4** crystallized in monoclinic space group $P2_1/n$ (Table S1). The cationic part of **1**, $[Dy_4L_4(\mu_2\text{-}N_3)_2]^{2+}$, contains a dimer building block, $\{Dy_2\}$, which can be clearly identified (Figure 1, left) and acts as an asymmetric unit of **1**; the bond lengths and angles are shown in Tables S2 and S3. The asymmetric unit contains two Dy^{III} ions, denoted as Dy1 and Dy2 with a distance of 3.6593(5) Å, linked by two bridging phenolic O atoms (O3 and O10) and a bridging azide N atom (N3) respectively. Two $\{Dy_2\}$ units are welded by four flexible $-(CH_2)_4-$ chains at the termini of four L^{2-} ligands, giving rise to the final supramolecular cluster **1** (Figures 1 and S1). Furthermore, the crystal structure contains two counter NO_3^- anions and some solvent molecules in the lattice. Each Dy^{III} ion is nine-coordinated and located at slightly distorted spherical tricapped trigonal prism (D_{3h}, Dy1) and spherical capped square antiprism (C_{4v}, Dy2) coordination geometry with in total N_3O_6 donors from the coordination pockets of three L^{2-} ligands (N_2O_6) and a N_3^- anion (N), respectively (Figure S2, Table S4). The Dy−N and Dy−O distances fall in the range of 2.487(6)−2.620(6) Å and 2.188(5)−2.698(5) Å, respectively. The distances among Dy···Dy which reside on both sides of the ligand are in the range of 8.450−9.093 Å. The structural study reveals that **1** possesses a quadruple-stranded helicate arrangement very similar to previously reported $[La_4L'_4(NO_3)](NO_3)_3]$.[7d] Four Dy^{III} ions were encapsulated in the center with an arrangement of a tortile rectangle; at the same time, all the ligands wrap around the Dy^{III} ions in an well-ordered and helical manner, forming the quadruple-stranded helicate supramolecular skeleton with a scale of 13.5 × 16.7 Å^2.

Owing to exceptional flexibility and manifold coordination functionality of H_2L, accompanied by little variations in reaction conditions results in some more larger and interesting structures (**2**−**4**). Indeed, accompanying the ligand rearrangement, the two triple-stranded helicates were linked by two transverse ligands instead of a quadruple-stranded helicate arrangement as in case of **1**; thus, a dual triple-stranded helicate supramolecular structure $[Dy_8L_8(\mu_2\text{-}CH_3OH)_4]Cl_8\cdot 6CH_3OH\cdot 14H_2O$ (**2**) is obtained. More surprisingly, when the ligands aligned in a "whirlpool"-like fashion, rather than helicate, two novel $[Dy_{12}L_{12}(\mu_2\text{-}OH)_2(OH)_6(CH_3O)_2](NO_3)_2\cdot 2CH_3OH\cdot 14H_2O$ (**3**) and $[Dy_{12}L_{12}(\mu_2\text{-}OH)_2(NO_3)_2(OH)_3(CH_3O)](NO_3)_4\cdot 22H_2O$ (**4**) "octahedron" cagelike structures are obtained.

Yet again, the asymmetric unit of complex **2** contains a half of the total molecule, which comprises four Dy^{III} ions, four doubly deprotonated ligands, two coordinated methanol molecules, and some Cl^- anions and solvent molecules in the lattice (Figures S3 and S4); the bond lengths and angles are shown in Table S5 and S6. Then two asymmetric fragments, $[Dy_4L_4(\mu_2\text{-}CH_3OH)_2]^{4+}$, were installed together to form the ultimate inner core $[Dy_8L_8(\mu_2\text{-}CH_3OH)_4]^{8+}$ (Figure 2, left). The two triple-strand skeletons $\{Dy_4\}$ were welded by two ligands in a latitudinal direction with a size of 21.6 × 20.6 Å^2 instead of arranging in quadruple-stranded helicate as described above, which not only possess a dual triple-stranded helicate supramolecular structure but also behave as a twisted gridlike structure with an obvious cavity (Figure 2, right).

In both triple-stranded helicates, the arrangement of Dy^{III} ions is approximate to a twisted parallelogram, where the effective lengths of sides are 3.693(12), 3.689(13), 9.223(24), and 9.346(24) Å, respectively. Moreover, the Dy^{III} ions in the two triple-stranded helicate substructures have a relatively longer separation (transverse distance: 10.608(27)-12.497(28) Å. In view of integral structure, the $\{Dy_2\}$ units located at the four vertices of the grid framework, and each occupied one side of the four ligands by coordinating to the donor atoms. At the

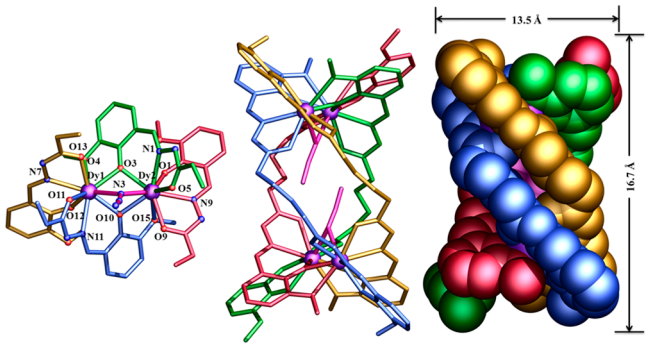

Figure 1. Asymmetric unit of **1** (left). Only one side termini of four L^{2-} trapping a dimer $\{Dy_2\}$ along with intrabridging through azide (N_3) have been shown; the crystallographic structure of the cationic part of **1**, $[Dy_4L_4(\mu_2\text{-}N_3)_2]^{2+}$ (middle), the space-filling model (right), highlighting the tight arrangement of the helicate. The purple, red, and blue spheres represent Dy, O, and N, respectively. Hydrogen atoms, solvent molecules, and counterions have been omitted for clarity.

DOI: 10.1021/acs.inorgchem.8b03249
Inorg. Chem. XXXX, XXX, XXX−XXX

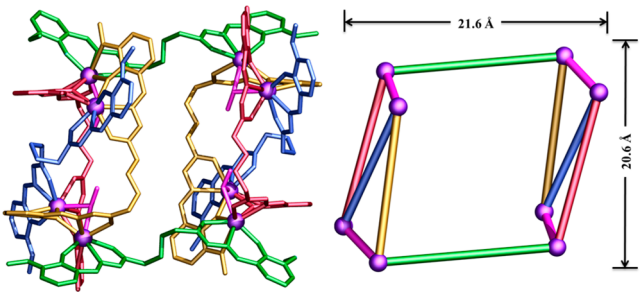

Figure 2. Crystallographic structure of complex **2** (left). The arrangement of ligands and Dy^{III} ions are highlighted (right); pink highlights bridged methanol. Hydrogen atoms, solvent molecules, and counterions have been omitted for clarity.

same time, the Dy^{III} ions of $\{Dy_2\}$ unit are held together by two bridging phenolic O atoms of ligand (O8, O24 or O11, O13) and a bridging alcoholic O atom (O16 or O25). Each Dy^{III} ion is nine-coordinated and surrounded by two N atoms incorporate with seven O atoms, coming from three L^{2-} and a methanol. The coordination geometry of Dy^{III} ions are distorted spherical capped square antiprism (C_{4v}, Dy1 and Dy4) and spherical tricapped trigonal prism (D_{3h}, Dy2 and Dy3), respectively (Figure S5), as determined by the program SHAPE[23] (Table S7). The Dy−N and Dy−O distances span the range of 2.174(11)−2.732(12) Å and 2.477(17)−2.577(14) Å, respectively. The intramolecular Dy···Dy separations which residing on both sides of the ligands are in the range of 9.223(24)−11.298(25) Å.

In contrast to **1** and **2**, the structure of **3** was found to be a dodecanuclear dysprosium cluster as shown in Figures 3 and S6. Single-crystal structural data analysis revealed that the each asymmetric unit $[Dy_6L_6(\mu_2\text{-}OH)(OH)_3(CHO)]^+$ was constructed by the coordination action of six Dy^{III} ions with six doubly deprotonated ligands and the number of terminal coordination anions (Figures S7 and S8); the bond lengths and angles are shown in Table S8 and S9. Two asymmetric units are welded together by four ligands, giving rise to a unique cagelike $[Dy_{12}L_{12}(\mu_2\text{-}OH)_2(OH)_6(CH_3O)_2]^{2+}$ core with a twisted octahedral cavity. The solvent molecules and counterions of crystallization were observed in the lattice to stabilize the structure. From the structural point of view, eight ligands can be described as the edges of the "octahedron" cagelike structure in which six $\{Dy_2\}$ subunits are connected through the termini of ligands via coordination bonds. The longitudinal Dy1 and Dy2 possess distorted spherical tricapped trigonal prism (D_{3h}) and spherical capped square antiprism (C_{4v}) geometry, respectively (Figure S9, Table S10). Both were bridged by two phenolic O atoms (O16 and O22) and a hydroxyl O atom (O45), respectively. The rest of the coordination sites were occupied by N_2O_4 donors coming from three L^{2-}. This type of $\{Dy_2\}$ unit was wrapped around by one side of the four ligands in a "whirlpool"-like fashion to further form a $\{Dy_2\}$ pivot (Figure S10). However, the other side of four ligands were occupied by four latitudinal $\{Dy_2\}$ (Dy3 and Dy4 or Dy5 and Dy6) units via NO_2 or NO_3 donors. Each latitudinal $\{Dy_2\}$ unit contains an eight-coordinated Dy^{III} ion (Dy4 or Dy6) and a nine-coordinated Dy^{III} ion (Dy3 or Dy5), which were linked by two bridging phenolic O atoms (O25, O28 or O8, O11) from the NO_2 and NO_3 donors mentioned above. Four latitudinal $\{Dy_2\}$ units act as latitudinal pivots and connect two longitudinal $\{Dy_2\}$ pivots from top and bottom, forming an octahedral cage. Simultaneously, the eight-coordinated Dy4 and Dy6 centers in the latitudinal direction possess the OH^- or CH_3O^- to fulfill the coordination number with the distorted triangular dodecahedron (D_{2d}) and biaugmented trigonal prism (C_{2v}) coordination geometry, respectively (Table S10). The nine-coordinated Dy3 and Dy5 centers in the latitudinal direction possess distorted spherical capped square antiprism (C_{4v}) coordination geometry. All Dy−O and Dy−N distances in the range of 2.138(5)−2.783(4) Å and 2.438(5)−2.590(4) Å, respectively, the adjacent distances of Dy_2···Dy_2 are in the range of 7.581(12)−11.641(14) Å.

The structure of nearly isoskeletal, dodecanuclear complex **4** was obtained, as shown in Figures 4 and S11. Although reminiscent to the overall core topology of **3**, there are still some conspicuous variances that merit further investigation. Complex **4** crystallizes in the monoclinic space group $P2_1/n$ (Table S1) instead of $C2/c$ (as in the case of **1**−**3**), which possesses the inner core molecule, $[Dy_{12}L_{12}(\mu_2\text{-}OH)_2(NO_3)_2(OH)_3(CH_3O)]^{4+}$. Comparatively, **3** and **4** show slight variances among their bond lengths and angles (for detail see Tables S11 and S12). In **4**, all Dy−O and Dy−N distances are in the range of 2.140−2.818 Å and 2.494−2.643

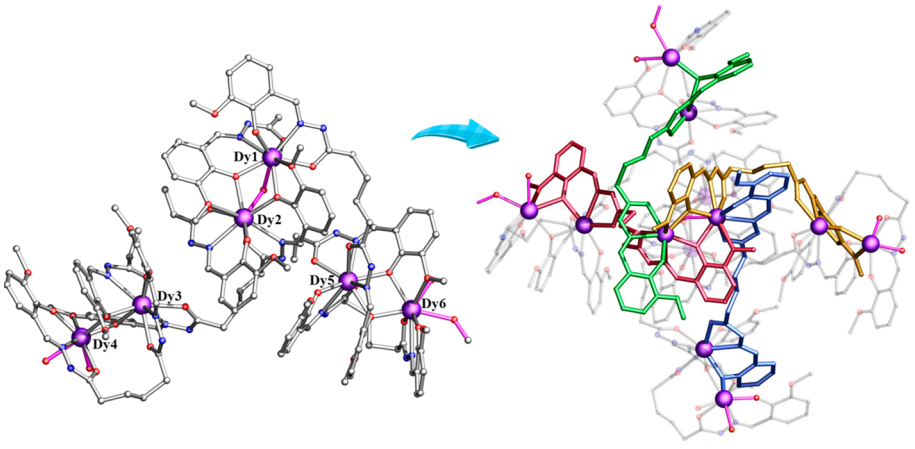

Figure 3. Asymmetric unit (left) and crystallographic structure (right) of complex **3**; the terminal coordination anions are described in pink. The "whirlpool"-like arrangement is highlighted. The purple, red, and blue spheres represent Dy, O, and N, respectively. Hydrogen atoms, solvent molecules, and counterions have been omitted for clarity.

DOI: 10.1021/acs.inorgchem.8b03249
Inorg. Chem. XXXX, XXX, XXX−XXX

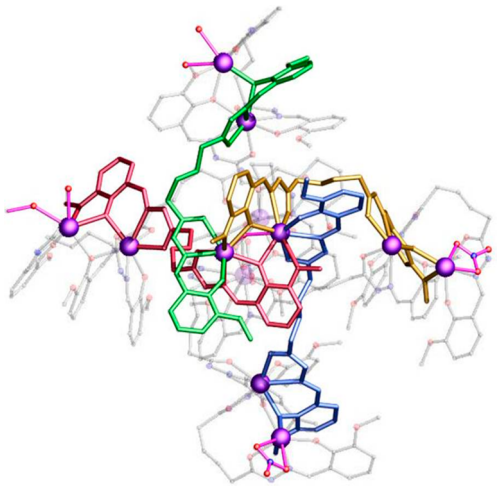

Figure 4. Crystallographic structure of complex **4**; the "whirlpool"-like arrangement is highlighted. The terminal coordination anions are described in pink. The purple, red, and blue spheres represent Dy, O, and N, respectively. Hydrogen atoms, solvent molecules, and counterions have been omitted for clarity.

Å, respectively. In addition, the eight-coordinated Dy^{III} ions (Dy4, Dy6, Dy10, and Dy12) in the latitudinal direction are all completed by several terminal coordination anions NO_3^-, OH^-, or CH_3O^- instead of OH^- or CH_3O^- as for complex **3** and adopt similar N_3O_6 spheres (Figure S12). The coordination geometry of all Dy^{III} ions are distorted spherical tricapped trigonal prism (D_{3h}, Dy1 and Dy7), spherical capped square antiprism (C_{4v}, Dy2, Dy3, Dy5, Dy8, Dy9, and Dy11), and biaugmented trigonal prism (C_{2v}, Dy4, Dy6, Dy10, and Dy12), respectively (Figure S13 and Table S13).

Magnetic Properties. Variable-temperature direct-current (dc) magnetic susceptibility measurements were performed on freshly prepared polycrystalline samples of all four complexes in a temperature range of 2−300 K under a static magnetic field of 0.1 T. The $\chi_M T$ (in which χ_M is molar magnetic susceptibility) versus T plots are presented in Figure 5. The

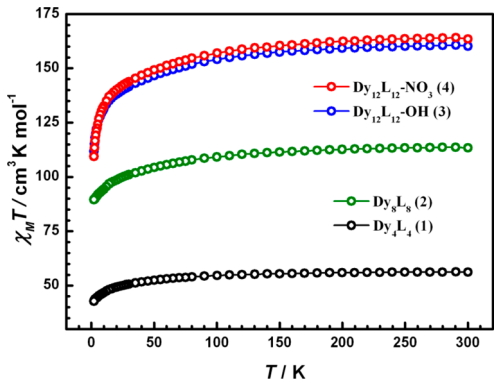

Figure 5. Temperature dependence of the $\chi_M T$ products for complexes **1**−**4** at 1 kOe between 2 and 300 K.

observed $\chi_M T$ values at room temperature are 56.24, 113.42, 160.22, and 163.53 cm^3 K mol^{-1} for complexes **1**−**4**, respectively, which are consistent with the theoretical values of 56.68, 113.36, 170.04 cm^3 K mol^{-1}, expected for Dy^{III}_4, Dy^{III}_8, and Dy^{III}_{12} (g = 4/3 of the $^6H_{15/2}$ ground state of the Dy^{III} ion) independent spin-only Dy^{III} ions, respectively. With the decrease of temperature, the $\chi_M T$ values of four complexes remain almost constant over the range 300−140 K. Below this temperature, the $\chi_M T$ products decrease gradually until 30 K, and then rapidly drop and reach the minimum values of 42.84, 91.59, 111.87, and 109.49 cm^3 K mol^{-1} at 2 K for complexes **1**−**4**, respectively. The decrease of $\chi_M T$ profiles may arise from the progressive excited depopulation of stark sublevel and/or non-negligible intra- or intermolecular antiferromagnetic interactions between the Dy^{III} ions.

The field dependence of the isothermal magnetization measurements were performed on complexes **1**−**4** at low-temperatures (1.9−5 K). The data are shown as magnetization (M) versus field (H) plots in Figure S14. The values of the M products rise abruptly at low fields, and then reach 22.58, 44.54, 63.18, and 61.86 μ_B until 70 kOe for four complexes at 1.9 K, respectively, without any sign of saturation, consistent with an obvious of magnetic anisotropy and/or low-lying excited states for Dy^{III}-containing systems. Moreover, the M versus H/T plots are not superimposed on a single master curve, which also indicates the presence of magnetic anisotropy and/or low-lying excited states.

With the aim to probe the dynamic magnetic behavior of complexes **1**−**4**, the ac magnetic susceptibility measurements were completed under zero/nonzero Oe applied dc fields. The temperature (T) or frequency (ν) dependence of in-phase (χ') and out-of-phase (χ'') ac magnetic susceptibilities were plotted. For complex **1**, no obvious out-of-phase (χ'') susceptibility signals were observed, even the temperature down to 1.9 K under 0 Oe applied dc field (Figure S15). Strikingly, the temperature-dependent χ'' signal (only in the low temperatures region) is strongly enhanced by a 800 Oe applied dc field, which, however, absence of the full peak with maximum, highlighting only slow magnetic relaxation behavior (Figure S16). Furthermore, similar out-of-phase (χ'') susceptibility behavior were discovered for **2** and **3** under a 0 Oe dc field (Figures S17 and S18), which suggests the presence of possible stronger quantum tunneling of magnetization (QTM) at low temperature, as described in some lanthanide-containing polynuclear systems.[16c] By contrast, a divergence of dynamic behavior was observed in complex **4**, as shown in Figure 6. In 0 Oe applied dc field, a series of obvious full peaks can be easily detected in the frequency-dependent susceptibility measurements below 20 K and the range of 1−1488 Hz. As the temperature is decreased, a clear shift of the χ'' peak maxima toward the low frequency region was observed, which is typical for SMM behavior.

To further decipher the magnetic characteristic of complex **4**, the relaxation times were extracted from fitting the frequency-dependent magnetic susceptibility data in the range of 1.9−20 K using the generalized Debye model, but the signal peaks are so wide that the extracting deviate from the developing track of data, especially in low-temperature region (Figure S19), only giving a poor result. Fitting the relaxation times versus temperatures (τ versus T^{-1} plots, Figure 7, top) with multiple relaxation processes using

$$\tau_{obs}^{-1} = \tau_{QTM}^{-1} + CT^n + \tau_0^{-1} \exp\left(\frac{-U_{eff}}{T}\right) \quad (1)$$

where τ_{QTM}^{-1}, CT^n and $\tau_0^{-1} \exp(-U_{eff}/k_BT)$ represent the Quantum tunneling, Raman, and Orbach relaxation processes, respectively, gave a cursory estimated effective energy barrier to magnetization reversal U_{eff} of 52 K (≈36 cm^{-1}) and pre-exponential factor $\tau_0 = 2.55 \times 10^{-6}$ s. There are merely a few

DOI: 10.1021/acs.inorgchem.8b03249
Inorg. Chem. XXXX, XXX, XXX−XXX

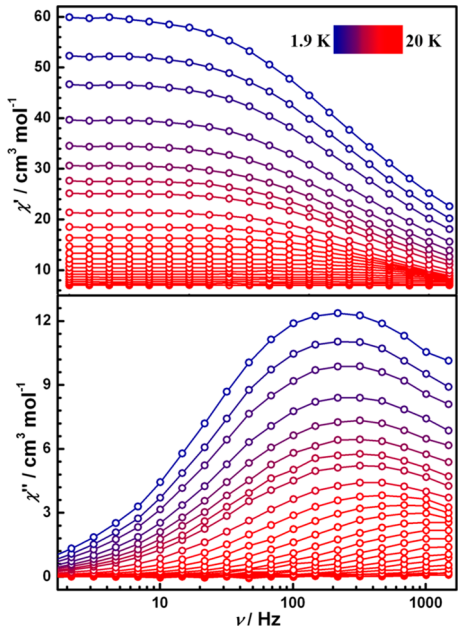

Figure 6. Frequency dependence of the in-phase (χ') (top) and out-of-phase (χ'') (bottom) ac-magnetic susceptibilities for complex **4** under a 0 dc field.

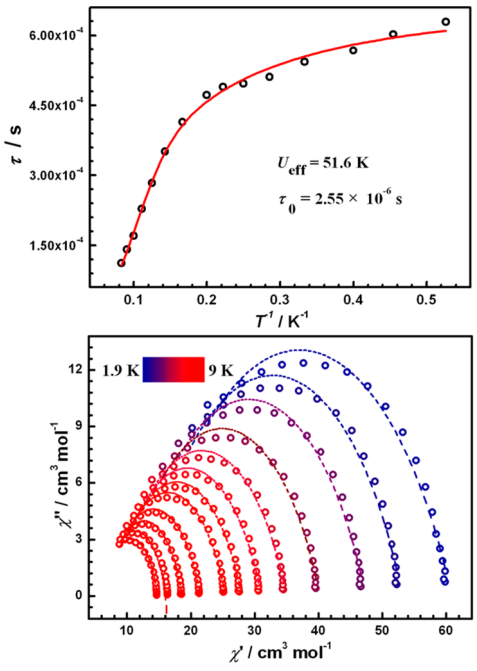

Figure 7. Magnetization relaxation time, τ, versus T^{-1} for **4** (top) and the Cole−Cole diagrams (bottom) under a 0 Oe dc field. The lines correspond to the best fit.

pure Dy^{III}-based metallosupramolecular systems having such a higher nuclearity that belong to this family of SMMs with effective energy barrier.

The semicircular Cole−Cole diagram of complex **4** was plotted via χ'' versus χ' from 1.9 to 9 K, as shown in Figure 7 (bottom). The collected data is fitted by a generalized Debye model, yielding α values are in the range of 0.19−0.36, which as expected suggested a relatively wide distribution of relaxation time constants for complex **4**. The χ'' signal shoulders being relatively more wider with the poor fit suggests the coalescence of the two peaks, indicating the possible presence of two relaxation processes.[24] Indeed, the isothermal frequency-dependent out-of-phase component of the susceptibility can be nicely simulated by two relaxation processes (Figure S20). Fitting the relaxation times and temperatures with the multiple relaxation processes yields the effective energy barriers (U_{eff}) of 64 K (≈44 cm^{-1}; $\tau_0 = 2.42 \times 10^{-6}$ s) and 33 K (≈23 cm^{-1}; $\tau_0 = 1.10 \times 10^{-5}$ s) for the SR and FR, respectively (Figure S21). Meanwhile, the Cole−Cole diagram was fit by two relaxation processes, which gives a perfect coincide (especially in the low temperature region), yielding α values in the ranges of 0.07−0.18 (FR) and 0.11−0.32 (SR), respectively (Figure S22). In addition, to make a reasonable comparison, we plotted the $\ln(\chi''/\chi')$ versus $1/T$ curves of complexes **1**−**3** and extracted U_{eff} of 2.5, 1.4, and 0.7 K, respectively (Figures S23−S25), by applying the Debye equation:[25]

$$\ln\left(\frac{\chi''}{\chi'}\right) = \ln(\omega\tau_0) + \frac{E_a}{k_B T} \quad (2)$$

As well-known, the subtle differences in structural features have far-reaching influence on the magnetic performance. Indeed, the absence of SMM behavior in complexes **1**−**3** is likely to attribute to QTM process within the ground exchange state. Fortunately, we turn on the SMM behavior by decorating the experimental conditions of $\{Dy_{12}\}$-acylhydrazone complex in a way that does not alter the core structure and the nature of faint intramolecular magnetic interactions. Nevertheless, the local coordination environments produce a slight modulation around Dy^{III} centers, as presented in Tables S10 and S13 and Figures S9 and S13. Especially for Dy4 in complex **3**, the symmetrical environment were modified from D_{2d} to C_{2v}. Indispensably, the other coordination geometry of Dy^{III} ions also possess a slight variation. From the standpoint of magnetostructural correlations, for pure Dy^{III}-based with SMM behavior, the unique magnetic characteristic mainly origins from single-ion anisotropy, which is extraordinarily sensitive to slight distortion of the symmetry geometry. Therefore, such structural differences resulting from the adjustment of coordination environments in the Dy^{III} centers and further influence the magnetic performance.

CONCLUSIONS

In summary, we designed and successfully synthesized a novel dihydrazone ligand H_2L with extraordinary pliability. This characteristic of ligand imparts a significant advantage to chelate Dy^{III} ions and create various topological supramolecular structures. Accordingly, a novel dysprosium based quadruple-stranded helicate, $[Dy_4L_4(\mu_2\text{-}N_3)_2](NO_3)_2 \cdot 6CH_3OH \cdot 2H_2O$ (**1**) has been obtained. Furthermore, by implementing the strategically synthetic variations a dual triple-stranded helicate $[Dy_8L_8(\mu_2\text{-}CH_3OH)_4]Cl_8 \cdot 6CH_3OH \cdot 14H_2O$ (**2**) and two novel "octahedron" cagelike $[Dy_{12}L_{12}(\mu_2\text{-}OH)_2(OH)_6(CH_3O)_2](NO_3)_2 \cdot 2CH_3OH \cdot 14H_2O$ (**3**) and $[Dy_{12}L_{12}(\mu_2\text{-}OH)_2(NO_3)_2(OH)_3(CH_3O)](NO_3)_4 \cdot 22H_2O$ (**4**) supramolecular structures have been synthesized. This strategy provides a vast range for interesting topological structures where strategically a little variation in reaction conditions, engaging the same metal−ligand combination can potentially results in drastic changes toward the final desired structures.

Moreover, complexes **1**−**3** only exhibit slow magnetic relaxation behavior. In contrast, the typical SMM behavior

DOI: 10.1021/acs.inorgchem.8b03249
Inorg. Chem. XXXX, XXX, XXX−XXX

was turned on for complex **4** at 0 Oe applied dc field benefiting from the modification of the local coordination environments around Dy^{III} ions, which is a rare case that possesses to such a number of nuclears in Dy^{III}-SMMs family. The interesting discovery plays an important role to develop new strategies toward developing Ln-supramolecular structure and molecule-based magnet. Simultaneously, constructing the novel supramolecular structures with SMM behavior could be further explored by using such kind of flexible ligands as a linker. As part of our research interests, the extension of this work to other linkers and Ln-ions based series is currently in progress for widening the range of outstanding properties.

■ ASSOCIATED CONTENT

Supporting Information

The Supporting Information is available free of charge on the ACS Publications website at DOI: 10.1021/acs.inorgchem.8b03249.

Experimental sections, crystallographic data, selected bond lengths and angles, SHAPE analysis, crystal structure, magnetic measurements (PDF)

Accession Codes

CCDC 1866900−1866903 contain the supplementary crystallographic data for this paper. These data can be obtained free of charge via www.ccdc.cam.ac.uk/data_request/cif, or by emailing data_request@ccdc.cam.ac.uk, or by contacting The Cambridge Crystallographic Data Centre, 12 Union Road, Cambridge CB2 1EZ, UK; fax: +44 1223 336033.

■ AUTHOR INFORMATION

Corresponding Authors

*E-mail: yuy@ciac.ac.cn (Y.Y.).
*E-mail: cezlliu@imu.edu.cn (Z.L.).
*E-mail: tang@ciac.ac.cn (J.T.).

ORCID

Zhiliang Liu: 0000-0003-3917-6014
Jinkui Tang: 0000-0002-8600-7718

Notes

The authors declare no competing financial interest.

■ ACKNOWLEDGMENTS

This work was supported by the National Natural Science Foundation of China (Grants 21525103, and 21871247). B.A. is grateful for the support of the CAS-TWAS President's Fellowship. J.T. gratefully acknowledges support of the Royal Society-Newton Advanced Fellowship (NA160075).

■ REFERENCES

(1) (a) Caulder, D. L.; Raymond, K. N. Supermolecules by Design. *Acc. Chem. Res.* **1999**, *32*, 975−982. (b) Smulders, M. M. J.; Riddell, I. A.; Browne, C.; Nitschke, J. R. Building on architectural principles for three-dimensional metallosupramolecular construction. *Chem. Soc. Rev.* **2013**, *42*, 1728−1754. (c) Lindoy, L. F.; Park, K.-M.; Lee, S. S. Metals, macrocycles and molecular assemblies - macrocyclic complexes in metallo-supramolecular chemistry. *Chem. Soc. Rev.* **2013**, *42*, 1713−1727. (d) Brown, C. J.; Toste, F. D.; Bergman, R. G.; Raymond, K. N. Supramolecular Catalysis in Metal−Ligand Cluster Hosts. *Chem. Rev.* **2015**, *115*, 3012−3035.

(2) (a) He, Z.; Jiang, W.; Schalley, C. A. Integrative self-sorting: a versatile strategy for the construction of complex supramolecular architecture. *Chem. Soc. Rev.* **2015**, *44*, 779−789. (b) Chen, L.; Chen, Q.; Wu, M.; Jiang, F.; Hong, M. Controllable Coordination-Driven Self-Assembly: From Discrete Metallocages to Infinite Cage-Based Frameworks. *Acc. Chem. Res.* **2015**, *48*, 201−210. (c) Roberts, D. A.; Pilgrim, B. S.; Nitschke, J. R. Covalent post-assembly modification in metallosupramolecular chemistry. *Chem. Soc. Rev.* **2018**, *47*, 626−644.

(3) Vyas, V. S.; Haase, F.; Stegbauer, L.; Savasci, G.; Podjaski, F.; Ochsenfeld, C.; Lotsch, B. V. A tunable azine covalent organic framework platform for visible light-induced hydrogen generation. *Nat. Commun.* **2015**, *6*, 8508.

(4) Lewis, J. E. M.; Beer, P. D.; Loeb, S. J.; Goldup, S. M. Metal ions in the synthesis of interlocked molecules and materials. *Chem. Soc. Rev.* **2017**, *46*, 2577−2591.

(5) Gil-Ramírez, G.; Leigh, D. A.; Stephens, A. J. Catenanes: Fifty Years of Molecular Links. *Angew. Chem., Int. Ed.* **2015**, *54*, 6110−6150.

(6) Thorp-Greenwood, F. L.; Kulak, A. N.; Hardie, M. J. An infinite chainmail of M_6L_6 metallacycles featuring multiple Borromean links. *Nat. Chem.* **2015**, *7*, 526.

(7) (a) Piguet, C.; Borkovec, M.; Hamacek, J.; Zeckert, K. Strict self-assembly of polymetallic helicates: the concepts behind the semantics. *Coord. Chem. Rev.* **2005**, *249*, 705−726. (b) Zhu, X.; He, C.; Dong, D.; Liu, Y.; Duan, C. Cerium-based triple-stranded helicates as luminescent chemosensors for the selective sensing of magnesium ions. *Dalton Trans* **2010**, *39*, 10051−10055. (c) Aroussi, B. E.; Zebret, S.; Besnard, C.; Perrottet, P.; Hamacek, J. Rational Design of a Ternary Supramolecular System: Self-Assembly of Pentanuclear Lanthanide Helicates. *J. Am. Chem. Soc.* **2011**, *133*, 10764−10767. (d) Wang, B.; Zang, Z.; Wang, H.; Dou, W.; Tang, X.; Liu, W.; Shao, Y.; Ma, J.; Li, Y.; Zhou, J. Multiple Lanthanide Helicate Clusters and the Effects of Anions on Their Configuration. *Angew. Chem., Int. Ed.* **2013**, *52*, 3756−3759. (e) Greenfield, J. L.; Rizzuto, F. J.; Goldberga, I.; Nitschke, J. R. Self-Assembly of Conjugated Metallopolymers with Tunable Length and Controlled Regiochemistry. *Angew. Chem., Int. Ed.* **2017**, *56*, 7541−7545. (f) Greenfield, J. L.; Evans, E. W.; Di Nuzzo, D.; Di Antonio, M.; Friend, R. H.; Nitschke, J. R. Unraveling Mechanisms of Chiral Induction in Double-Helical Metallopolymers. *J. Am. Chem. Soc.* **2018**, *140*, 10344−10353.

(8) (a) Wang, Y.-T.; Cui, A.-L.; Shen, D.-Z.; Kou, H.-Z. High-spin tetranuclear iron(III) grids: Synthesis, crystal structure and magnetic properties. *Polyhedron* **2013**, *52*, 970−975. (b) Wang, Y.-T.; Li, S.-T.; Wu, S.-Q.; Cui, A.-L.; Shen, D.-Z.; Kou, H.-Z. Spin Transitions in Fe(II) Metallogrids Modulated by Substituents, Counteranions, and Solvents. *J. Am. Chem. Soc.* **2013**, *135*, 5942−5945. (c) Wu, J.; Zhao, L.; Guo, M.; Tang, J. Constructing supramolecular grids: from 4f square to 3d-4f grid. *Chem. Commun.* **2015**, *51*, 17317−17320. (d) Wu, J.; Zhao, L.; Zhang, L.; Li, X.-L.; Guo, M.; Tang, J. Metallosupramolecular Coordination Complexes: The Design of Heterometallic 3d−4f Gridlike Structures. *Inorg. Chem.* **2016**, *55*, 5514−5519. (e) Wu, J.; Zhao, L.; Zhang, L.; Li, X.-L.; Guo, M.; Powell, A. K.; Tang, J. Macroscopic Hexagonal Tubes of 3 d−4 f Metallocycles. *Angew. Chem., Int. Ed.* **2016**, *55*, 15574−15578. (f) Li, X.-L.; Wu, J.; Zhao, L.; Shi, W.; Cheng, P.; Tang, J. End-to-end azido-pinned interlocking lanthanide squares. *Chem. Commun.* **2017**, *53*, 3026−3029. (g) Dhers, S.; Mondal, A.; Aguilà, D.; Ramírez, J.; Vela, S.; Dechambenoit, P.; Rouzières, M.; Nitschke, J. R.; Clérac, R.; Lehn, J.-M. Spin State Chemistry: Modulation of Ligand pKa by Spin State Switching in a [2 × 2] Iron(II) Grid-Type Complex. *J. Am. Chem. Soc.* **2018**, *140*, 8218−8227.

(9) (a) Jansze, S. M.; Cecot, G.; Wise, M. D.; Zhurov, K. O.; Ronson, T. K.; Castilla, A. M.; Finelli, A.; Pattison, P.; Solari, E.; Scopelliti, R.; Zelinskii, G. E.; Vologzhanina, A. V.; Voloshin, Y. Z.; Nitschke, J. R.; Severin, K. Ligand Aspect Ratio as a Decisive Factor for the Self-Assembly of Coordination Cages. *J. Am. Chem. Soc.* **2016**, *138*, 2046−2054. (b) Musser, A. J.; Neelakandan, P. P.; Richter, J. M.; Mori, H.; Friend, R. H.; Nitschke, J. R. Excitation Energy Delocalization and Transfer to Guests within $M^{II}_4L_6$ Cage Frameworks. *J. Am. Chem. Soc.* **2017**, *139*, 12050−12059. (c) Rizzuto, F. J.; Nitschke, J. R. Stereochemical plasticity modulates cooperative binding in a $Co^{II}_{12}L_6$ cuboctahedron. *Nat. Chem.* **2017**, *9*, 903. (d) Pilgrim, B. S.; Roberts, D. A.; Lohr, T. G.; Ronson, T. K.;

DOI: 10.1021/acs.inorgchem.8b03249
Inorg. Chem. XXXX, XXX, XXX−XXX

Nitschke, J. R. Signal transduction in a covalent post-assembly modification cascade. *Nat. Chem.* **2017**, *9*, 1276. (e) Li, X.-Z.; Zhou, L.-P.; Yan, L.-L.; Yuan, D.-Q.; Lin, C.-S.; Sun, Q.-F. Evolution of Luminescent Supramolecular Lanthanide $M_{2n}L_{3n}$ Complexes from Helicates and Tetrahedra to Cubes. *J. Am. Chem. Soc.* **2017**, *139*, 8237−8244.

(10) Lu, Z.; Knobler, C. B.; Furukawa, H.; Wang, B.; Liu, G.; Yaghi, O. M. Synthesis and Structure of Chemically Stable Metal-Organic Polyhedra. *J. Am. Chem. Soc.* **2009**, *131*, 12532−12533.

(11) (a) Zhao, L.; Wei, J.; Zhang, J.; He, C.; Duan, C. Encapsulation of a Quinhydrone Cofactor in the Inner Pocket of Cobalt Triangular Prisms: Combined Light-Driven Reduction of Protons and Hydrogenation of Nitrobenzene. *Angew. Chem.* **2017**, *129*, 15486−15490. (b) Jing, X.; Yang, Y.; He, C.; Chang, Z.; Reek, J. N. H.; Duan, C. Control of Redox Events by Dye Encapsulation Applied to Light-Driven Splitting of Hydrogen Sulfide. *Angew. Chem.* **2017**, *129*, 11921−11925. (c) Zhao, L.; Wei, J.; Lu, J.; He, C.; Duan, C. Renewable Molecular Flasks with NADH Models: Combination of Light-Driven Proton Reduction and Biomimetic Hydrogenation of Benzoxazinones. *Angew. Chem.* **2017**, *129*, 8818−8822.

(12) (a) Ramsay, W. J.; Rizzuto, F. J.; Ronson, T. K.; Caprice, K.; Nitschke, J. R. Subtle Ligand Modification Inverts Guest Binding Hierarchy in $M^{II}_8L_6$ Supramolecular Cubes. *J. Am. Chem. Soc.* **2016**, *138*, 7264−7267. (b) Percástegui, E. G.; Mosquera, J.; Nitschke, J. R. Anion Exchange Renders Hydrophobic Capsules and Cargoes Water-Soluble. *Angew. Chem., Int. Ed.* **2017**, *56*, 9136−9140. (c) Rodríguez, J.; Mosquera, J.; Couceiro, J. R.; Nitschke, J. R.; Vázquez, M. E.; Mascareñas, J. L. Anion Recognition as a Supramolecular Switch of Cell Internalization. *J. Am. Chem. Soc.* **2017**, *139*, 55−58. (d) Zhang, D.; Ronson, T. K.; Mosquera, J.; Martinez, A.; Nitschke, J. R. Selective Anion Extraction and Recovery Using a $Fe^{II}_4L_4$ Cage. *Angew. Chem., Int. Ed.* **2018**, *57*, 3717−3721.

(13) (a) Zhao, L.; Qu, S.; He, C.; Zhang, R.; Duan, C. Face-driven octanuclear cerium(iv) luminescence polyhedra: synthesis and luminescent sensing natural saccharides. *Chem. Commun.* **2011**, *47*, 9387−9389. (b) Hamacek, J.; Poggiali, D.; Zebret, S.; Aroussi, B. E.; Schneider, M. W.; Mastalerz, M. Building large supramolecular nanocapsules with europium cations. *Chem. Commun.* **2012**, *48*, 1281−1283. (c) He, C.; Wang, J.; Zhao, L.; Liu, T.; Zhang, J.; Duan, C. A photoactive basket-like metal-organic tetragon worked as an enzymatic molecular flask for light driven H2 production. *Chem. Commun.* **2013**, *49*, 627−629.

(14) (a) Bünzli, J.-C. G.; Piguet, C. Lanthanide-Containing Molecular and Supramolecular Polymetallic Functional Assemblies. *Chem. Rev.* **2002**, *102*, 1897−1928. (b) Benelli, C.; Gatteschi, D. Magnetism of Lanthanides in Molecular Materials with Transition-Metal Ions and Organic Radicals. *Chem. Rev.* **2002**, *102*, 2369−2388. (c) Woodruff, D. N.; Winpenny, R. E. P.; Layfield, R. A. Lanthanide Single-Molecule Magnets. *Chem. Rev.* **2013**, *113*, 5110−5148. (d) Zhang, P.; Guo, Y.-N.; Tang, J. Recent advances in dysprosium-based single molecule magnets: Structural overview and synthetic strategies. *Coord. Chem. Rev.* **2013**, *257*, 1728−1763. (e) Zhang, P.; Zhang, L.; Tang, J. Lanthanide single molecule magnets: progress and perspective. *Dalton Trans* **2015**, *44*, 3923−3929.

(15) Jing, X.; He, C.; Yang, Y.; Duan, C. A Metal−Organic Tetrahedron as a Redox Vehicle to Encapsulate Organic Dyes for Photocatalytic Proton Reduction. *J. Am. Chem. Soc.* **2015**, *137*, 3967−3974.

(16) (a) Chen, P.; Li, H.; Sun, W.; Tang, J.; Zhang, L.; Yan, P. Crystallization of triple- and quadruple-stranded dinuclear bis-*β*-diketonate-Dy(III) helicates: single molecule magnetic behavior. *CrystEngComm* **2015**, *17*, 7227−7232. (b) Li, H.; Chen, P.; Sun, W.; Zhang, L.; Yan, P. Solvent triggered structural diversity of triple-stranded helicates: single molecular magnets. *Dalton Trans* **2016**, *45*, 3175−3181. (c) Habib, F.; Long, J.; Lin, P.-H.; Korobkov, I.; Ungur, L.; Wernsdorfer, W.; Chibotaru, L. F.; Murugesu, M. Supramolecular architectures for controlling slow magnetic relaxation in field-induced single-molecule magnets. *Chem. Sci.* **2012**, *3*, 2158−2164.

(17) (a) Ishikawa, N.; Sugita, M.; Ishikawa, T.; Koshihara, S.-y.; Kaizu, Y. Lanthanide Double-Decker Complexes Functioning as Magnets at the Single-Molecular Level. *J. Am. Chem. Soc.* **2003**, *125*, 8694−8695. (b) Tang, J.; Hewitt, I.; Madhu, N. T.; Chastanet, G.; Wernsdorfer, W.; Anson, C. E.; Benelli, C.; Sessoli, R.; Powell, A. K. Dysprosium Triangles Showing Single-Molecule Magnet Behavior of Thermally Excited Spin States. *Angew. Chem., Int. Ed.* **2006**, *45*, 1729−1733. (c) Tian, H.; Wang, M.; Zhao, L.; Guo, Y. N.; Guo, Y.; Tang, J.; Liu, Z. A Discrete Dysprosium Trigonal Prism Showing Single-Molecule Magnet Behaviour. *Chem. - Eur. J.* **2012**, *18*, 442−445. (d) Wu, J.; Li, X.-L.; Guo, M.; Zhao, L.; Zhang, Y.-Q.; Tang, J. Realization of toroidal magnetic moments in heterometallic 3d-4f metallocycles. *Chem. Commun.* **2018**, *54*, 1065−1068.

(18) (a) Rinehart, J. D.; Long, J. R. Exploiting single-ion anisotropy in the design of f-element single-molecule magnets. *Chem. Sci.* **2011**, *2*, 2078−2085. (b) Zhang, P.; Zhang, L.; Wang, C.; Xue, S.; Lin, S. Y.; Tang, J. Equatorially coordinated lanthanide single ion magnets. *J. Am. Chem. Soc.* **2014**, *136*, 4484−7.

(19) Guo, F.-S.; Day, B. M.; Chen, Y.-C.; Tong, M.-L.; Mansikkamäki, A.; Layfield, R. A. Magnetic hysteresis up to 80 K in a dysprosium metallocene single-molecule magnet. *Science* **2018**, *362*, 1400−1403.

(20) Mondal, A. K.; Jena, H. S.; Malviya, A.; Konar, S. Lanthanide-Directed Fabrication of Four Tetranuclear Quadruple Stranded Helicates Showing Magnetic Refrigeration and Slow Magnetic Relaxation. *Inorg. Chem.* **2016**, *55*, 5237−5244.

(21) (a) Ke, H.; Xu, G.-F.; Zhao, L.; Tang, J.; Zhang, X.-Y.; Zhang, H.-J. A Dy10 Cluster Incorporates Two Sets of Vertex-Sharing Dy3 Triangles. *Chem. - Eur. J.* **2009**, *15*, 10335−10338. (b) Miao, Y.-L.; Liu, J.-L.; Leng, J.-D.; Lin, Z.-J.; Tong, M.-L. Chloride templated formation of $\{Dy_{12}(OH)_{16}\}^{20+}$ cluster core incorporating 1,10-phenanthroline-2,9-dicarboxylate. *CrystEngComm* **2011**, *13*, 3345−3348. (c) Tian, H.; Bao, S.-S.; Zheng, L.-M. Cyclic single-molecule magnets: from the odd-numbered heptanuclear to a dimer of heptanuclear dysprosium clusters. *Chem. Commun.* **2016**, *52*, 2314−2317.

(22) Asghari Lalami, N.; Hosseini Monfared, H.; Noei, H.; Mayer, P. Binuclear vanadium(V) complexes of bis(aryl)adipohydrazone: synthesis, spectroscopic studies, crystal structure and catalytic activity. *Transition Met. Chem.* **2011**, *36*, 669.

(23) (a) Zabrodsky, H.; Peleg, S.; Avnir, D. Continuous symmetry measures. 2. Symmetry groups and the tetrahedron. *J. Am. Chem. Soc.* **1993**, *115*, 8278−8289. (b) Alvarez, S.; Alemany, P.; Casanova, D.; Cirera, J.; Llunell, M.; Avnir, D. Shape maps and polyhedral interconversion paths in transition metal chemistry. *Coord. Chem. Rev.* **2005**, *249*, 1693−1708. (c) Ruiz-Martínez, A.; Casanova, D.; Alvarez, S. Polyhedral Structures with an Odd Number of Vertices: Nine-Coordinate Metal Compounds. *Chem. - Eur. J.* **2008**, *14*, 1291−1303.

(24) (a) Guo, Y.-N.; Xu, G.-F.; Gamez, P.; Zhao, L.; Lin, S.-Y.; Deng, R.; Tang, J.; Zhang, H.-J. Two-Step Relaxation in a Linear Tetranuclear Dysprosium(III) Aggregate Showing Single-Molecule Magnet Behavior. *J. Am. Chem. Soc.* **2010**, *132*, 8538−8539. (b) Zhang, L.; Jung, J.; Zhang, P.; Guo, M.; Zhao, L.; Tang, J.; Le Guennic, B. Site-Resolved Two-Step Relaxation Process in an Asymmetric Dy_2 Single-Molecule Magnet. *Chem. - Eur. J.* **2016**, *22*, 1392−1398. (c) Wu, J.; Lin, S.-Y.; Shen, S.; Li, X.-L.; Zhao, L.; Zhang, L.; Tang, J. Probing the magnetic relaxation and magnetic moment arrangement in a series of Dy_4 squares. *Dalton Trans* **2017**, *46*, 1577−1584.

(25) Jiménez, J.-R.; Díaz-Ortega, I. F.; Ruiz, E.; Aravena, D.; Pope, S. J. A.; Colacio, E.; Herrera, J. M. Lanthanide Tetrazolate Complexes Combining Single-Molecule Magnet and Luminescence Properties: The Effect of the Replacement of Tetrazolate N3 by *β*-Diketonate Ligands on the Anisotropy Energy Barrier. *Chem. - Eur. J.* **2016**, *22*, 14548−14559.

DOI: 10.1021/acs.inorgchem.8b03249
Inorg. Chem. XXXX, XXX, XXX−XXX